New Mexico Geological Society

Downloaded from: https://nmgs.nmt.edu/publications/guidebooks/76



Fault-Stratigraphic Relationships Across the Sand Hill and San Ysidro Fault Zones, Northwestern Albuquerque Basin, New Mexico: Implications for Paleoseismic Studies of Low-Slip-Rate Faults in Semiarid Settings

Sean D. Connell, Daniel J. Koning, and Andrew P. Jochems
2026, pp. 277-290. https://doi.org/10.56577/FFC-76.277

in:

Geology of the Albuquerque Region - Fall Field Conference 2026, Connell, Sean D.; Koning, Daniel J.;, New Mexico Geological Society 76th Annual Fall Field Conference Guidebook, 452 p. https://doi.org/10.56577/FFC-76

This is one of many related papers that were included in the 2026 NMGS Fall Field Conference Guidebook.

Annual NMGS Fall Field Conference Guidebooks

Every fall since 1950, the New Mexico Geological Society (NMGS) has held an annual Fall Field Conference that explores some region of New Mexico (or surrounding states). Always well attended, these conferences provide a guidebook to participants. Besides detailed road logs, the guidebooks contain many well written, edited, and peer-reviewed geoscience papers. These books have set the national standard for geologic guidebooks and are an essential geologic reference for anyone working in or around New Mexico.

Free Downloads

NMGS has decided to make peer-reviewed papers from our Fall Field Conference guidebooks available for free download. This is in keeping with our mission of promoting interest, research, and cooperation regarding geology in New Mexico. However, guidebook sales represent a significant proportion of our operating budget. Therefore, only *research papers* are available for download. *Road logs*, *mini-papers*, and other selected content are available only in print for recent guidebooks.

Copyright Information

Publications of the New Mexico Geological Society, printed and electronic, are protected by the copyright laws of the United States. No material from the NMGS website, or printed and electronic publications, may be reprinted or redistributed without NMGS permission. Contact us for permission to reprint portions of any of our publications.

One printed copy of any materials from the NMGS website or our print and electronic publications may be made for individual use without our permission. Teachers and students may make unlimited copies for educational use. Any other use of these materials requires explicit permission.

This page is intentionally left blank to maintain order of facing pages.

New Mexico Geological Society Guidebook, 76th Fall Field Conference, 2026, p. 277–290, https://doi.org/10.56577/FFC-76.277

FAULT-STRATIGRAPHIC RELATIONSHIPS ACROSS THE SAND HILL AND SAN YSIDRO FAULT ZONES, NORTHWESTERN ALBUQUERQUE BASIN, NEW MEXICO: IMPLICATIONS FOR PALEOSEISMIC STUDIES OF LOW-SLIP-RATE FAULTS IN SEMIARID SETTINGS

SEAN D. CONNELL[1], DANIEL J. KONING[1], AND ANDREW P. JOCHEMS[2]

[1]New Mexico Bureau of Geology and Mineral Resources, 801 Leroy Pl, Socorro, NM 87801; sean.connell@nmt.edu
[2]New Mexico Environment Department, 5401 Watson Drive SE, Albuquerque, NM 87106

Abstract—Locally extensive stratigraphic wedges in the northwestern Albuquerque Basin of New Mexico form on the hanging walls of normal faults and preserve records of syntectonic accommodation under low rates of slip. The Sand Hill and San Ysidro fault zones exert strong controls on the deposition of the Plio–Pleistocene Ceja Formation and overlying deposits. The Ceja Formation thickens basinward and is eroded across the bounding Mio–Pliocene Rincones paleosurface and the lower Pleistocene Llano de Albuquerque geomorphic surface, with attenuated footwall sections and more complete hanging-wall successions. Mapping of a 26-m (85-ft)-thick stratigraphic proximal hanging-wall succession along the Calabacillas segment of the San Ysidro fault documents at least 18 stacked paleosol-bounded subunits developed on top of the Llano de Albuquerque geomorphic surface. These deposits record episodic sediment accumulation punctuated by prolonged intervals of landscape stability and pedogenic carbonate development since 1.8 Ma and prior to 1.3 Ma. The high frequency of paleosol stacking in the Calabacillas succession indicates a strong climatic influence on local deposition and preservation, a factor that has generally been underappreciated in previous paleoseismic studies. These characteristics indicate that tectonic accommodation interacts with climatically modulated sediment supply to produce soil-bounded packages where tectonic events can be obscured by paleoclimatic variations. Although comparisons with paleoclimate proxies suggest strong climatic influences, limited geochronologic control precludes direct correlation of the wedge stratigraphy with specific ground-rupture events. Additional dating is necessary to strengthen paleoseismic interpretations. Integrating soil–stratigraphic relationships, sediment provenance, geomorphic context, and geochronology can more reliably distinguish rupture-related deposition from climatically driven sedimentation in eolian-prone, low-slip-rate settings.

INTRODUCTION

Geomorphically stable landforms provide useful stratigraphic datum planes to assess cumulative fault displacement over Pleistocene timescales. In the Albuquerque Basin of New Mexico, intrabasinal normal faults generally exhibit low long-term slip rates, ranging from 0.01 to 0.1 mm/yr (10–100 m/Myr), with recurrence intervals on the order of 10^4–10^5 years (U.S. Geological Survey, 2024). These relatively long timescales overlap major modes of Pleistocene climatic variability, including, but not limited to, precessional (~19 and ~23 kyr), obliquity (~41 kyr), and eccentricity-driven (~100 kyr) cyclicity (e.g., Lisiecki and Raymo, 2015). This apparent temporal correspondence raises the possibility that climatically driven variability in sediment supply, eolian activity, effective moisture, and pedogenesis may obscure the stratigraphic expression of individual paleoearthquake events.

Eolian sedimentation and pedogenic processes influence the preservation and stratigraphic architecture of fault-proximal deposits in semiarid, low-slip-rate settings, complicating the direct inference of rupture frequency from stratigraphic packages alone. We examine this through (1) detailed stratigraphic mapping of the Calabacillas segment of the San Ysidro fault zone, (2) mapping of paleosols, and (3) comparison with paleoclimate proxies to evaluate depositional controls. This paper describes a faulted succession of Miocene and Pleistocene deposits of the syn-rift Santa Fe Group along the Ceja del Rio Puerco, a north-trending erosional escarpment that marks the eastern edge of the Rio Puerco Valley in the northwestern Albuquerque Basin (Fig. 1). We examine a well-exposed sedimentary wedge overlying the Ceja Formation on the hanging wall of the Calabacillas fault segment that covers an area of more than 60 km^2 (23 mi^2, unit QTc in Connell, 2006, 2008a).

Colluvial wedges form in response to tectonic activity or climatically driven hillslope instability. In tectonically active settings, hanging-wall wedge deposits can represent syntectonic, fault-controlled sedimentary accumulations that thicken and coarsen toward fault scarps, preserving a stratigraphic record of episodic displacement along basin-margin or intrabasinal structures (Fig. 2; Machette, 1978). Paleoseismic investigations typically treat these deposits as single-event horizons (e.g., McCalpin, 1996); however, colluvial wedges may also develop during climatic intervals that destabilize hillslopes and enhance sediment flux (e.g., Pederson et al., 2000, 2001). In semiarid settings, locally derived colluvial wedges may be obscured by eolian and sheetwash deposition. Subsequent pedogenic carbonate development can mask primary sedimentary structures and architecture, complicating the delineation of discrete surface-rupture events. In the Calabacillas fault succession, mapping of individual paleosol-bounded

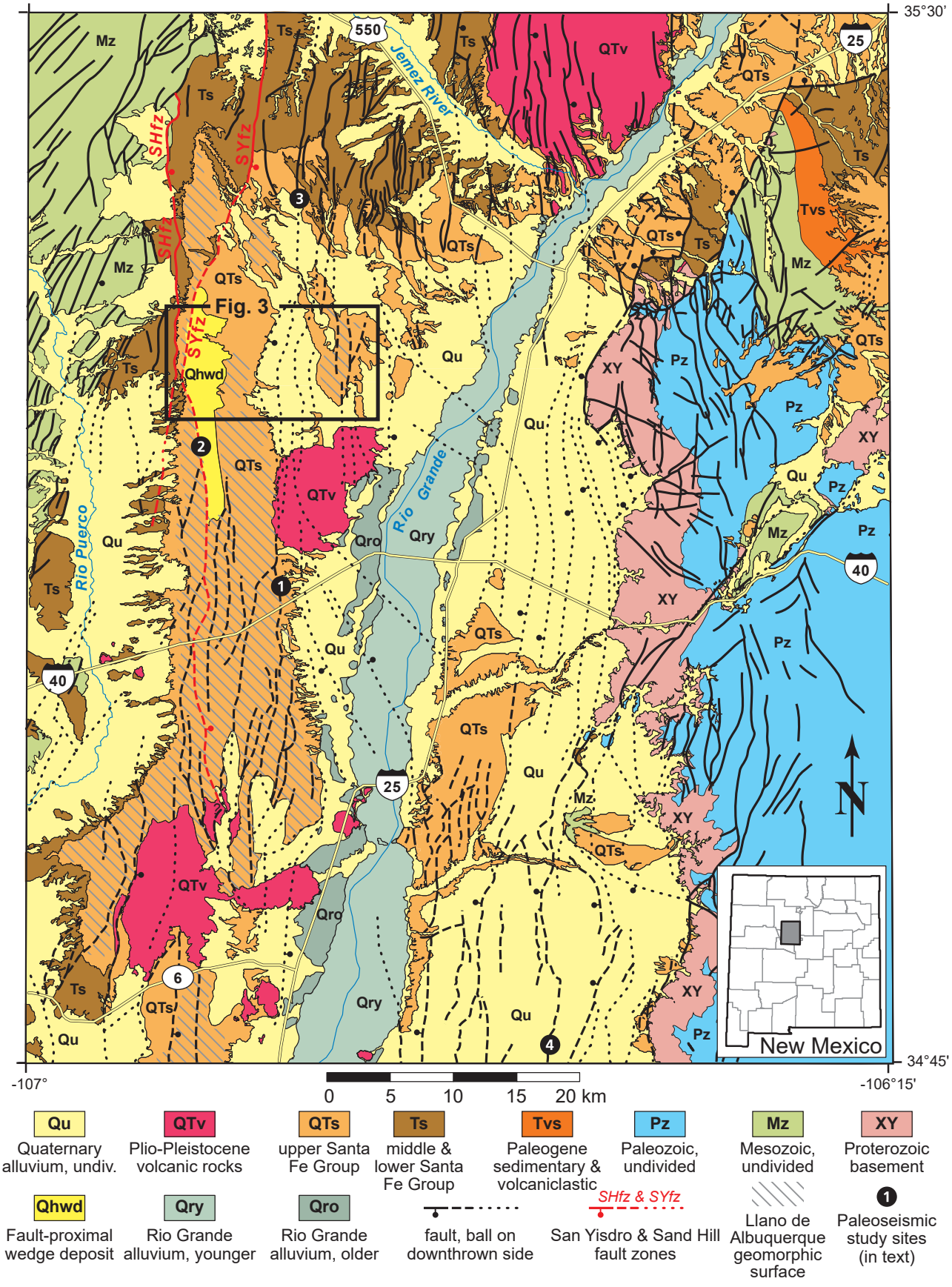


FIGURE 1. Generalized geologic map of the Albuquerque Basin (modified from Connell, 2004). The black box denotes the location of Figure 3. Black numbered circles denote localities described in text: (1) County Dump fault zone; (2) San Ysidro fault zone (SYfz); (3) Zia fault zone; and (4) Hubbell Springs fault zone. Traces of the Sand Hill fault zone (SHfz) and SYfz are depicted by red lines.

wedges suggests a major role for climatic cyclicity modulated by relatively low rates of vertical slip across the San Ysidro fault zone.

This study builds on previous paleoseismic investigations of intrabasinal faults in the Albuquerque area (Personius and Mahan, 2003; McCalpin et al., 2006, 2011; McCalpin, 2025) by integrating soil–stratigraphic analysis with outcrop mapping to resolve features that can be difficult to discern in trench-scale exposures. Paleoseismic studies of the County Dump, San Ysidro, and Zia fault zones show differences in fault geometry, segmentation, and geomorphic setting (Fig. 1). Along the Calabacillas fault segment, McCalpin et al. (2011) documented approximately 27 m (89 ft) of cumulative vertical displacement and identified at least four paleoearthquakes during late Pleistocene time. Individual events produced small vertical displacements (<0.5 m [1.6 ft]), yielding late Pleistocene slip rate estimates of 0.01–0.03 mm/yr (10–30 m/Myr) and recurrence intervals of ~10–20 kyr (McCalpin et al., 2011).

STRATIGRAPHY

Introduction

Exposures along the Ceja del Rio Puerco preserve composite fault-proximal wedges formed through incremental tectonic accommodation, erosion of uplifted blocks, localized deposition, and pedogenic stabilization. Wright (1946) first recognized syntectonic deposition across faults that were later mapped as the Sand Hill and San Ysidro fault zones (e.g., Connell, 2008a). Wright also documented systematic thickness variations and intraformational unconformities and described an accumulation of ~46 m (~150 ft) of stacked sand and gravel with at least 19 calcic paleosols that he interpreted as the product of repeated small fault displacements separated by prolonged intervals of landscape stability, soil formation, and burial (Wright, 1946).

We examine this faulted succession and document how the Sand Hill and San Ysidro zones preserve stratigraphic discordances and growth relationships, and contrast these observations with deposits on the proximal hanging wall of the Calabacillas segment of the San Ysidro fault, which contains a 26-m (85-ft)-thick succession that overlies the lower Pleistocene Llano de Albuquerque geomorphic surface. The Calabacillas fault wedge contains more than sixteen paleosol-bounded subunits dominated by eolian and sheetwash sand, with subordinate colluvial and alluvial facies (see below).

Ceja Formation

The Ceja Formation (upper Santa Fe Group) is a Plio–Pleistocene fluvial succession that unconformably overlies fluvial strata of the Miocene Arroyo Ojito Formation (middle Santa Fe Group; Connell, 2008b). The Ceja Formation is widespread across the western part of the Albuquerque Basin and consists of amalgamated fluvial channel-belt sand and gravel, and sandy sheetflood deposits derived from south–southeast-flowing tributary drainages sourced from the southeastern Colorado Plateau, Nacimiento Mountains, and Jemez Mountains (Connell, 2004). The Ceja Formation is divided into the Rio Puerco, Santa Ana Mesa, and Atrisco Members (Connell, 2008b). It is bounded above by the lower Pleistocene Llano de Albuquerque geomorphic surface (Machette, 1985) and below by the Mio–Pliocene Rincones paleosurface of Connell (2008b).

The Llano de Albuquerque geomorphic surface is a relict constructional surface marking the end of Ceja Formation aggradation, shortly after the Olduvai normal-polarity subchron (C2n.1n; Connell et al., 2013), and between 1.945–1.778 Ma (Gibbard and Head, 2020). Magnetostratigraphic correlations and radioisotopic dating of tephra and fluvially recycled pebbles constrain abandonment of the Llano de Albuquerque geomorphic surface to after 1.8 Ma and before 1.3 Ma (Connell et al., 2013). Paleosols developed on the Llano de Albuquerque geomorphic surface commonly exhibit pedogenic carbonate morphology ranging from stage III to III+ and, locally, stage IV development (Connell, 2008b). Pedogenic carbonate stages and soil descriptions follow Machette (1985) and references therein.

Fault-Proximal Hanging-Wall Wedge Deposits

Hanging-wall wedge deposits are syntectonic, fault-controlled accumulations that thicken and coarsen toward active fault scarps, recording episodic displacement along basin-bounding and intrabasinal structures (Fig. 2A). Deposits include scarp-derived colluvium, fissure fills, and alluvium from local strike-parallel drainages (e.g., Nelson, 1992). Sheetwash, rillwash, and eolian sediment typically blanket exposed fault scarps. Internal stratification commonly reflects individual surface faulting events, intervening periods of stability, and aggradation (e.g., McCalpin, 1996).

Fault wedges are composite geomorphic and stratigraphic features that include (1) initial scarp-derived colluvium, (2) slopewash and rilling associated with erosion of the newly exposed free face, and (3) locally extensive eolian and sheetwash that can obscure primary rupture-related deposits (Nelson, 1992; Personius and Mahan, 2003). Diagnostic indicators of surface faulting include fault-bounded colluvial wedges, basal erosional contacts, fissure fills, growth strata, lenses of scarp-derived debris, abrupt upward terminations of fault strands, and truncated paleosols (McCalpin, 1996). Following ground rupture, steep and freshly exposed topographic scarps rapidly collapse and are modified by rilling and erosion to form colluvial wedges. Preservation of discrete event horizons is facilitated by subsequent burial by younger colluvium, sheetwash, eolian sediment, and local stream and arroyo alluvium.

Fault-bounded colluvial wedges typically form immediately following ground-surface rupture as scarp-derived debris accumulates on the hanging walls of tectonically active faults (Fig. 2B–2F; Machette, 1978). An individual wedge deposit is a discrete sedimentary unit that represents a single depositional episode within a larger composite wedge succession defined by paleosols or other diastems. The influence of climate on sedimentation and erosion is widespread; however, at

the local hanging-wall wedge scale, the relative influence of erosion and deposition is expected to diminish away from the fault scarp (Fig. 2G).

In the Albuquerque Basin, hanging-wall wedges are preserved adjacent to intrabasinal faults, where they provide evidence for high-angle normal faulting, quantify discrete paleoseismic events, and have been used to constrain Pleistocene slip histories through integration of stratigraphic relations, soil morphologic development, and geochronologic datasets (Personius and Mahan, 2003; McCalpin et al., 2006, 2021; McCalpin, 2025). Because colluvial-wedge deposits may not represent single rupture events, more reliable interpretations can be achieved by carefully identifying event horizons and analyzing internal stratigraphy and sediment provenance to distinguish tectonically driven deposition from climatically modulated sediment pulses.

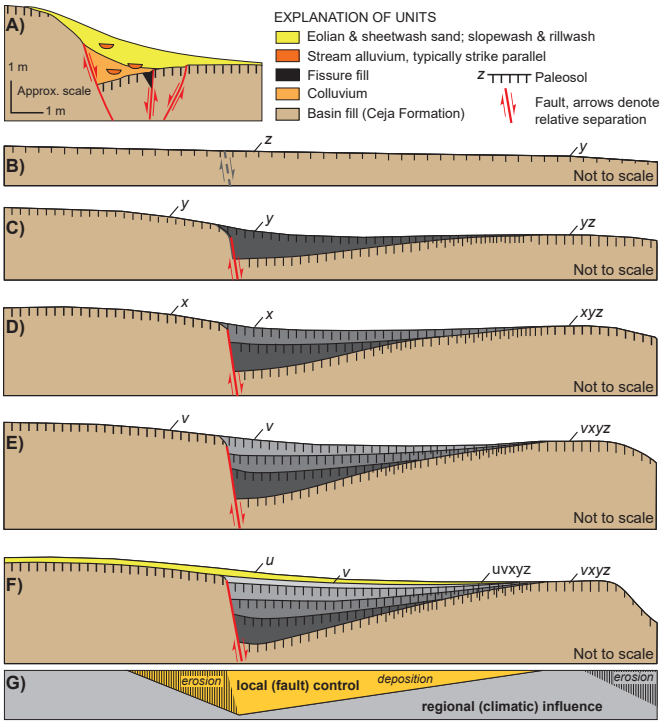


FIGURE 2. Diagram illustrating soil–stratigraphic conceptual model of fault-scarp colluvium modified from Machette (1978) and Nelson (1992). Individual subunits are defined by paleosols, represented by short vertical hachures. A: Sketch of scarp-proximal deposits, illustrating depositional relationships of a fault-adjacent colluvial wedge, local scarp-parallel alluvium, and blankets of sheetwash and eolian sediment that commonly mantle the fault scarp. B–F: Conceptual sequence illustrated by successive cross sections. B: Initial pre-fault conditions and development of soil z. C: A colluvial wedge forms on proximal hanging wall, followed by a period of relative quiescence, allowing soil y to form on the wedge top. Soil–morphological development increases away from the fault (denoted by soils yz). Panels D and E: Subsequent wedges and soils vxyz are produced by repetition of the process in panel C. F: Thin layer of eolian sand covering the scarp, forming cumulic (or composite) paleosols uvxyz, where covered by eolian sand, and vxyz where the surface is not mantled by younger sediment. G: Conceptual sketch illustrating the relative magnitudes of regional (climatic) and local (fault) controls on erosion, deposition, preservation, and soil formation. The length and spacing of vertical hachures infer the relative influence of erosional processes across the footwall and stream erosion on the distal hanging wall.

In semiarid basins, eolian processes are common, particularly where vegetation is sparse, and dust fluxes are high (Reheis et al., 2005). Personius and Mahan (2003) documented laterally continuous, paleosol-bounded sand sheets along the Hubbell Spring fault zone (see Fig. 1) that consist largely of windblown sediment mixed with scarp-derived debris. They interpreted these sand sheets as having been deposited immediately after surface-rupturing earthquakes, when coseismic scarps created local topographic traps that accumulated eolian sand on the proximal hanging wall. Individual 1–2-m (3–7-ft)-thick, paleosol-bounded deposits may approximate single events and provide indirect proxies for slip magnitude where distributed deformation, pedoturbation, and bioturbation can obscure interpretations of event stratigraphy (Personius and Mahan, 2003). Eolian-dominated depositional mechanisms contrast with the debris-rich colluvial wedges typical of many paleoseismic sites in the Basin and Range province (Nelson, 1992; Gray et al., 2022) and underscore the importance of incorporating paleoclimatic variability and geomorphic context when interpreting fault scarp stratigraphy.

Eolian Deposits

Eolian sediment discontinuously mantles cuestas and mesas in the western part of the Albuquerque Basin, commonly obscuring exposures of the Ceja Formation and Llano de Albuquerque geomorphic surface. Thin (<1–3 m [<3–10 ft]) eolian sand sheets and dunes are widespread and locally interbedded with paleosols in fault-controlled wedges (Connell, 2008a; Thompson et al., 2009). Eolian rim dunes are discontinuous moderate-relief features with crestlines that are up to ~15 m (~49 ft) high and parallel to the Ceja del Rio Puerco and the western edge of the Llano de Albuquerque geomorphic surface (Kelley, 1977). These dunes reflect enhanced deposition of fine- to medium-grained sand and silt where airflow decelerates across slope breaks (e.g., Pye and Tsoar, 2009). Rim dunes laterally grade into mixed eolian sheetwash deposits that are punctuated by weakly developed paleosols (Holliday et al., 2006; Hall et al., 2008).

Eolian successions are commonly punctuated by buried paleosols, demonstrating that net accumulation rates were episodic and separated by relatively long intervals of surface stability. Hall et al. (2008) reported multiple episodes of late Pleistocene and Holocene eolian deposition using optically stimulated luminescence (OSL) and radiocarbon dating. Below is a summary of eolian stratigraphy overlying the Llano de Albuquerque following Hall et al. (2008). Eolian sediment yielded radiocarbon and OSL ages of 2.6–1.3 ka. Areally extensive sheets of fine- to medium-grained sand are typically less than 1.4 m (5 ft) in thickness and contain paleosols exhibiting stage I pedogenic carbonate morphology that were deposited ~16–10 ka. Uppermost Pleistocene deposits unconformably overlie eolian and Ceja Formation strata. Older eolian deposits consist of silty sand with paleosols that exhibit stage II pedogenic carbonate morphology with an estimated OSL age of ~130 ka. Even older eolian deposits overlie the Ceja Formation

and exhibit stage III carbonate morphology with solution pipes filled with upper Pleistocene sediment.

FAULT–STRATIGRAPHIC RELATIONSHIPS

At least five proximal hanging-wall wedges are preserved along intrabasinal faults on the western end of Southern Boulevard (unit Qhwd; Fig. 3). Figure 3 illustrates how fault proximity and local depositional slopes control the distribution of fault wedges in the study area. Individual fault wedges are recognized as topographic inflections or steps across west-tilted faulted blocks exposing prominent white petrocalcic paleosols associated with the Llano de Albuquerque geomorphic surface described in Machette (1985). These wedges are difficult to observe in the field because they are commonly obscured by eolian, sheetwash, slopewash, and alluvial sediments.

Six stratigraphic sections were described across the Sand Hill and San Ysidro fault zones using available exposures and subsurface data (Figs. 3 and 4). Thicknesses of the Ceja, Arroyo Ojito, and Cerro Conejo Formations were interpreted from regional mapping and previous stratigraphic studies (Tedford and Barghoorn, 1999; Connell, 2008a, 2008b; Connell et al., 1999, 2013; Koning et al., 2026). These stratigraphic sections show basinward thickening of the Ceja Formation and an overall basinward decrease in the magnitude of the lacuna associated with the underlying Rincones paleosurface, a regionally mappable unconformity in the Albuquerque Basin (Connell, 2008b).

Figure 4 is a stratigraphic fence constructed along a nearly 12 km (7.5 mi) transect to illustrate the stratigraphic relationships between the Santa Fe Group and an overlying fault wedge associated with the Calabacillas segment of the San Yisdro fault zone. At Red Hill (RH-1), gravel and sand of the Rio Puerco Member of the Ceja Formation is locally scoured into sandstone and minor mudstone of the middle Miocene Cerro Conejo Formation on the footwall of the Sand Hill fault. On the hanging wall of the San Ysidro fault, approximately 2 km (1.25 mi) to the south at SG-2, is a slightly more complete but erosionally attenuated section of Rio Puerco and Atrisco Member deposits, both of which unconformably overlie an erosionally truncated section of the upper Miocene Arroyo Ojito Formation (Figs. 4 and 5). At SG-2, on the proximal hanging wall of the Sand Hill fault, the Rio Puerco Member scoured into the Atrisco Member, which overlies an erosionally truncated section of Navajo Draw Member with a slight angular unconformity (Fig. 6). This contact is disconformable at the CDRP-CL section of Connell et al. (2013), approximately 1.5 km (1 mi) to the southeast of SG-1 (Fig. 4).

Two sites along the proximal hanging wall of the San Ysidro fault document a thicker section of the Ceja Formation that unconformably overlies the Navajo Draw Member (Figs. 4 and 5). In the study area, this boundary is marked by a petrocalcic soil with stage III+ carbonate morphologic development (Connell et al., 2013). Eolian, alluvial, sheetwash, and colluvial deposits on proximal hanging wall are represented by stratigraphic sections SG-1 and SG-3 (Fig. 4). Nearly 5 km (3 mi) to the southeast, a 916 m (3,005 ft) groundwater exploration well (RG-67000) encountered approximately 82–137 m (269–450 ft) of sand, gravel, and silt forming an upward-coarsening succession that is typical of the Ceja Formation (Connell, 2006).

Calabacillas Fault Segment Hanging-Wall Wedge

A well-exposed fault-controlled proximal hanging-wall wedge succession (unit Qhwd) is preserved within an erosional amphitheater along the proximal hanging wall of the Calabacillas segment of the San Ysidro fault zone (Figs. 5, 7, and 8). The nearly 1 km (0.6 mi) of strike-parallel exposures along part of a ~20-km (~12-mi)-long, 3-km (2-mi)-wide wedge provide an exceptional view of fault-proximal stratigraphic relationships and sedimentation patterns. The amphitheater geometry permits physical correlation of individual paleosol-bounded units nearly 300 m (984 ft) away from the fault. To aid interpretation, a photogrammetric outcrop model was constructed using structure-from-motion modeling (e.g., Westoby et al., 2012). Paleosol-bounded subunits were traced across the outcrop face in Figure 8. Thicker soil-bounded intervals are marked by prominent white-capped ledges that exhibit stage III and III+ pedogenic carbonate morphology, whereas less strongly developed but laterally mappable paleosol-bounded units commonly exhibit stage I and II pedogenic carbonate morphology.

Two stratigraphic sections (SG-1 and SG-3) document a succession of proximal hanging-wall wedge deposits that overlie the Ceja Formation. Four lithologic units (units A–D) are shown on Figures 4 and 8. Paleosol-bounded subunits, many ~1 m (~3 ft) in thickness, were traced up to 300 m (984 ft) away from the fault, yielding an average depositional slope of <0.2°. Deposits are predominantly sand, silt, and mud, with sparse gravel. Comparison with gravel content and pedogenic carbonate data from Machette et al. (1997) supplemented outcrop mapping. Section 5 of Machette et al. (1997) contains fewer than 4% gravel, and paleosols contain up to ~35% calcium carbonate (Fig. 8).

Unit A consists of the upper part of the Rio Puerco Member of the Ceja Formation and forms the basal unit in sections SG-1 and SG-3 (Figs. 4, 8, and 9). Unit A contains very pale-brown, medium- to thick-bedded pebbly sand and medium-grained sand with sparse mudstone interbeds. The upper boundary of unit A is marked by at least two cumulic paleosols correlated to the Llano de Albuquerque geomorphic surface. A ~1-m (~3-ft)-thick, light gray, cross-stratified volcanic ash occurs approximately 24 m (79 ft) below the top of the Ceja Formation (the "Shooting Gallery" ash of Connell, 2008a, sample SA-11). At the time of collection, sanidine crystals separated from this ash were considered too fine grained to be dated by $^{40}Ar/^{39}Ar$ geochronology; tephrochronology did not yield correlations to known or dated ashes.

Units B and C contain at least 18 paleosols, marking multiple episodes of sedimentation and pedogenesis. Unit B is 14–16 m (46–52 ft)-thick and consists primarily of very fine- to medium-grained sand interbedded with scattered fine- to coarse-grained and pebbly sand lenses. It forms cliffs and contains at least 11 paleosols and at least 3 pebbly sand lenses. Paleosols exhibit stage II to III pedogenic carbonate

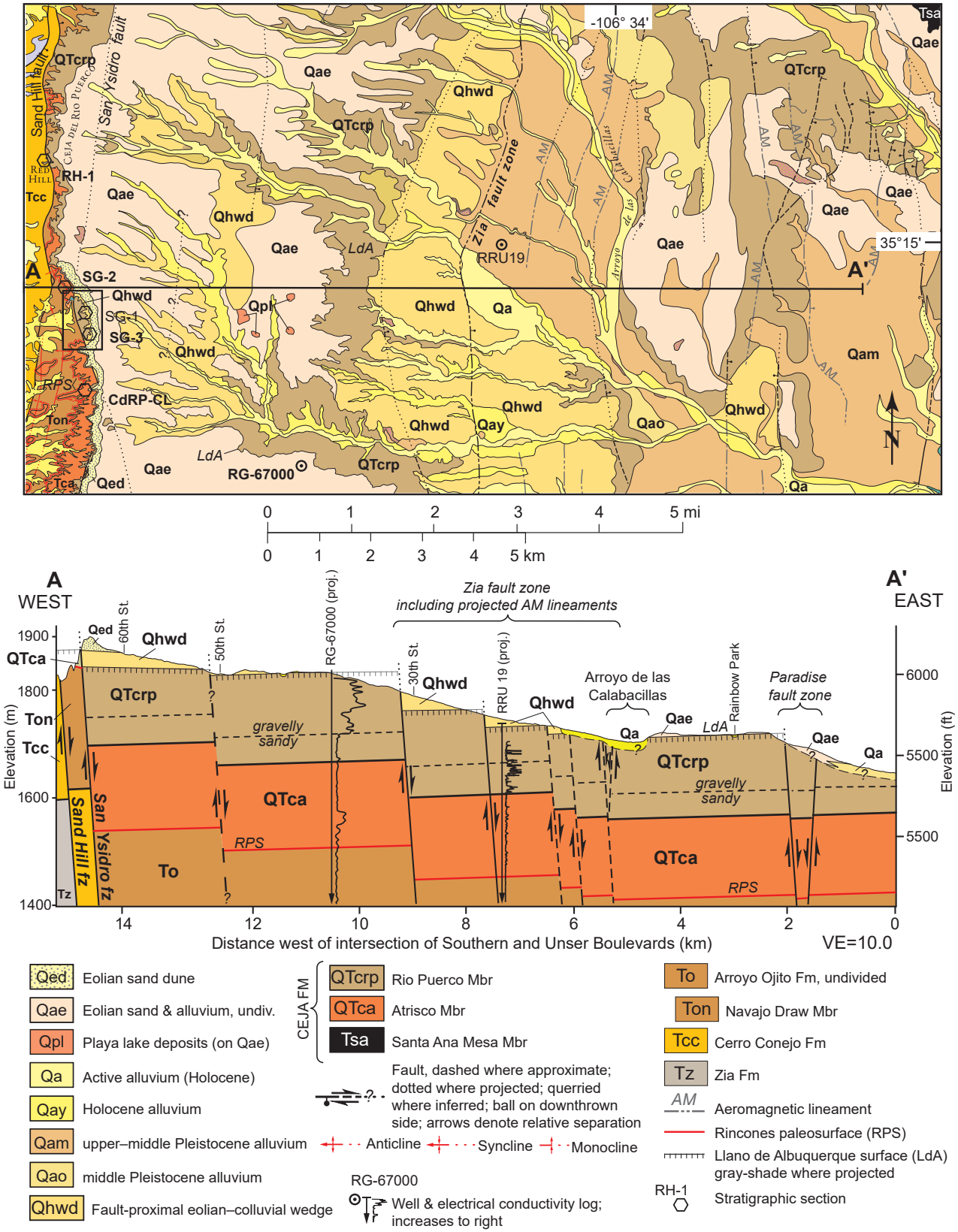


FIGURE 3. Geologic map highlighting areas where thick and laterally extensive hanging-wall wedge deposits (unit Qhwd) have been identified and a vertically exaggerated (VE=2.0) cross section along the western part of Southern Boulevard (map modified from Connell, 2006). The black box denotes the location of Figure 8. The Llano de Albuquerque geomorphic surface (LdA) marks the depositional top of the Plio–Pleistocene Ceja Formation (QTcrp). Stratigraphic sections described along the Ceja del Rio Puerco (CDRP) include RH-1, SG-1, SG-2, and SG-3. Stratigraphic section CDRP-CL was described by Connell et al. (2013). The Rincones paleosurface (RPS) defines the top of the upper Miocene Arroyo Ojito Formation (To). Surficial deposits include alluvium (Qa), eolian dune sand (Qed), and undivided sheetwash, alluvium, and eolian sand (Qae).

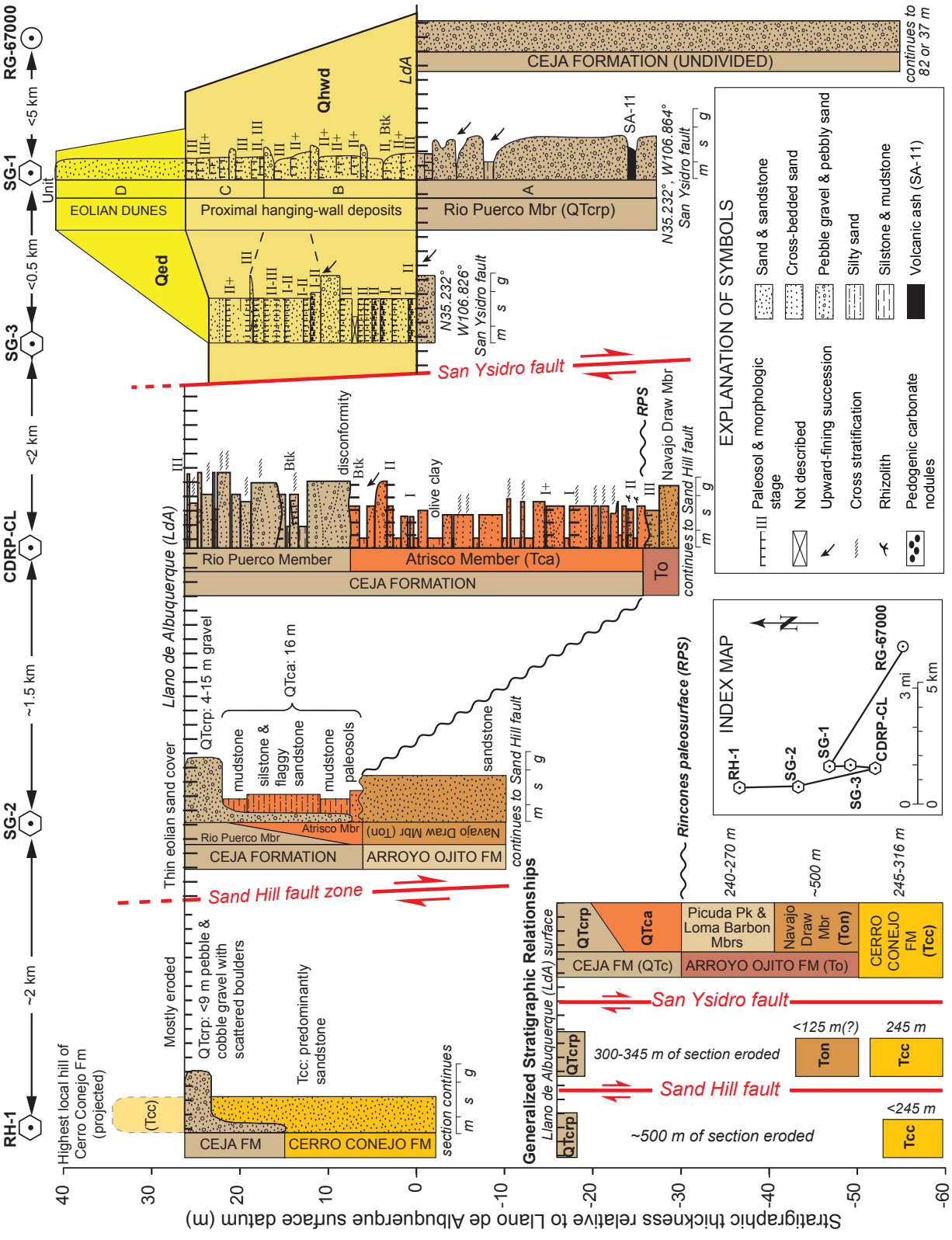


FIGURE 4. Stratigraphic relationships between the Ceja Formation and superjacent and subjacent deposits across the Sand Hill and San Ysidro fault zones. The fence diagram uses the Llano de Albuquerque geomorphic surface (LdA) as a stratigraphic datum, with unit Qhwd resting directly on it east of the San Ysidro fault. The Rincones paleosurface (RPS) forms a lower erosional boundary among stratigraphic sections on the footwall of the San Ysidro fault zone. The lower left part of the figure illustrates the magnitude of stratigraphic lacunae between fault blocks (Connell, 2004, 2008b; Connell et al., 1999; Koning et al., 2026). RG-67000 is a groundwater exploration well located nearly 5 km (3 mi) east of the San Ysidro fault, where it penetrated a thick and nearly complete stratigraphic section of the Ceja Formation (stratigraphic markers from Connell, 2006).

morphology, locally with Btk horizons identified by illuviated clay films on ped faces. The top of unit B forms a topographic ledge of calcium-carbonate cemented pebbly sand that is approximately 0.5 m (1.6 ft) in thickness.

Unit C overlies unit B and consists of ~10 m (~32 ft) of thin- to medium-bedded fine- to coarse-grained sand with scattered pebbly sand and sparse, thin- to medium-bedded mud. Sand is typically massive and locally pedoturbated and contains at least 7 paleosols. The upper contact forms a ~1-m (~3-ft)-thick ledge of sand capped by two overlapping (i.e., cumulic) paleosols displaying stage III to III+ pedogenic carbonate development.

Unit D is approximately 14 m (46 ft) in thickness and forms the uppermost deposit in the Calabacillas fault-wedge succession (Figs. 4 and 8). It consists of fine- to medium-grained, well-sorted sand preserved as eolian rim dunes along the Ceja del Rio Puerco. Unit D sand is structureless to weakly bedded and generally lacks strong pedogenic development, distinguishing it from the underlying paleosol-bearing units B and C. These poorly vegetated dunes indicate that eolian deposition continues to the present day.

DISCUSSION

Vertical stacking of multiple paleosol-bounded units within the Calabacillas hanging-wall wedge records repeated alternations between relatively brief depositional episodes and longer periods of relative landscape stability and pedogenic carbonate accumulation. Paleosols mark diastems that, as a whole, indicate relatively short but significant gaps in the stratigraphic succession. Geochronologic constraints indicate that deposition of this wedge succession began between 1.8 Ma and 1.3 Ma (Connell et al., 2013). Based on correlations to dated eolian deposits to the east and southeast of the study area, deposition continued until at least 0.13 Ma (Hall et al., 2008). Episodic eolian deposition reflects a composite history

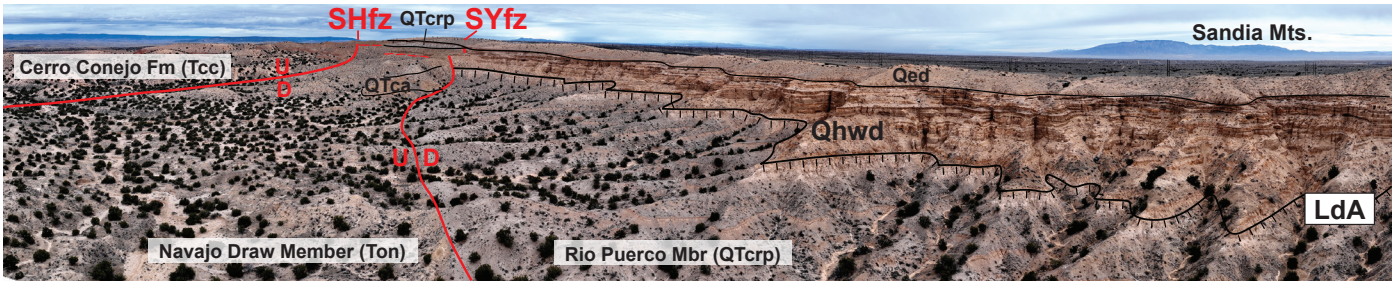


FIGURE 5. Photographic panorama looking north across an erosional amphitheater along the Ceja del Rio Puerco, showing the Calabacillas segment of the Sand Hill (SHfz) and San Ysidro (SYfz) fault zones (thick red lines), proximal hanging-wall deposits (unit Qhwd), Rio Puerco (QTcrp) and Atrisco (QTca) Members of the Ceja Formation, Navajo Draw Member (Ton) of the Arroyo Ojito Formation, and Cerro Conejo Formation (Tcc). The white layer at the top of the Rio Puerco Member marks the Llano de Albuquerque geomorphic surface (LdA). The thin dashed red line marks the location of the Rincones paleosurface. Eolian dune sand locally caps the rim of the Ceja del Rio Puerco.

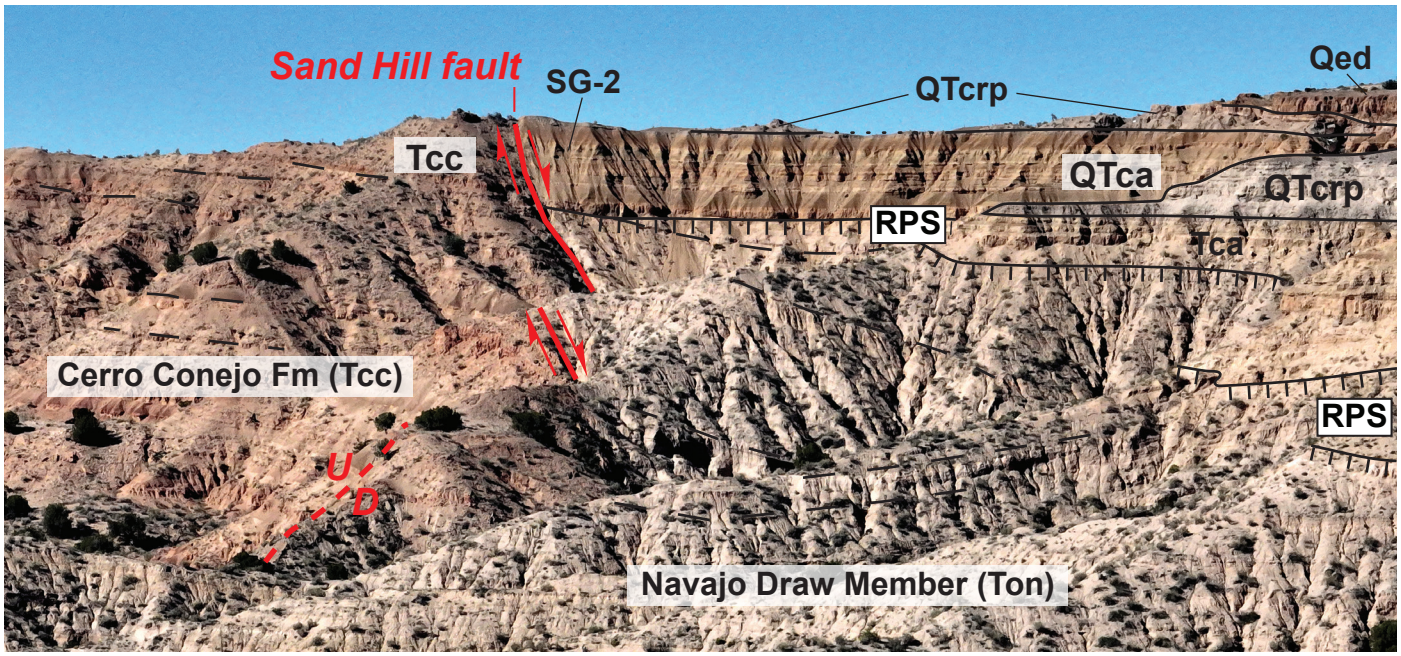


FIGURE 6. View north of Sand Hill fault and SG-2 stratigraphic section illustrating where the Sand Hill fault juxtaposes east-dipping, middle Miocene deposits of the Cerro Conejo Formation (Tcc, middle Santa Fe Group) against the Rio Puerco (QTcrp) and Atrisco (QTca) Members of the Plio–Pleistocene Ceja Formation (upper Santa Fe Group). The Atrisco Member unconformably overlies deposits of the Navajo Draw Member (Ton) of the upper Miocene Arroyo Ojito Formation (middle Santa Fe Group). The Mio–Pliocene Rincones paleosurface (RPS) marks the contact between the Ceja and Arroyo Ojito Formation.

of tectonic accommodation, climate-driven sediment supply, and pedogenesis.

Preservation of paleosol-bounded successions immediately east of the Calabacillas fault segment indicates that intrabasinal faulting remained active after the cessation of Ceja Formation deposition. In this context, fault-controlled accommodation locally disrupted regional sedimentation patterns, allowing continued sediment accumulation and soil development on the proximal hanging wall, while adjacent upland areas not directly influenced by local fault subsidence experienced either overall stability or erosion. This proximal hanging-wall fault-wedge succession contrasts regional depositional regimes with localized fault-controlled deposition of eolian and reworked sediments, thereby preserving climatic and tectonic signals in the stratigraphic record. The Ceja Formation reflects basin-scale fluvial deposition sourced primarily from southeast-flowing tributary systems to the ancestral Rio Grande; however, overlying hanging-wall wedge deposits contain eolian sand and locally derived sand and pebbly sand deposited by smaller-scale processes (e.g., sheetwash and rill-wash). This transition reflects both a cessation in regional fluvial sedimentation following abandonment of the Llano de Albuquerque geomorphic surface and the increased influence of localized tectonic accommodation generated by incremental vertical displacements across the San Ysidro fault zone.

The presence of numerous paleosols in a stratigraphic succession that spans over one million years of geologic time indicates that net sediment accumulation rates were relatively slow and episodic. Sediment delivery was repeatedly interrupted by prolonged intervals of relative geomorphic stability sufficient to allow significant pedogenic carbonate accumulation. These soil–stratigraphic relationships are consistent with post-Ceja landscapes becoming more susceptible to erosional modification and localized sediment trapping.

Climatic Modulation

The predominance of eolian sediment and calcic paleosols within the Calabacillas hanging-wall wedge indicates that wedge development may be modulated by climatic variability superimposed on localized tectonic accommodation. Along the Calabacillas fault segment, deposition above the Llano de Albuquerque geomorphic surface records the interaction of incremental fault displacement with climatically paced changes in sediment availability and landscape stability. Periods of relative aridity, prolonged surface stability, and variations in net sedimentation and preservation, likely corresponding to interglacial and interstadial intervals, favored pedogenic carbonate accumulation, forming stacked, laterally continuous paleosol-bounded subunits. In contrast, climatic transitions and glacial–interglacial boundary conditions can enhance dust production and sediment mobility through vegetation changes, exposure of sediment sources, hillslope destabilization, and stronger regional winds (e.g., Reheis et al., 2005). These processes promote the accumulation of thicker, vertically stacked eolian sand packages that onlap older paleosols. Ellwein et al. (2015) showed that substantial eolian deposition can occur during near- to full-glacial climate conditions (~32–20 ka), indicating that eolian deposition is not exclusively tied to climatic transitions. Eolian deposition may reflect colder, windier conditions that enhance sediment supply and transport capacity, rather than peak aridity (e.g., Ellwein et al., 2018).

Major orbitally driven climate variations imposed on this succession include the transition to more strongly eccentricity modulated (~100-kyr cycle) glaciations during middle (774–129 ka) and late Pleistocene (126–11.7 ka) times (e.g., Farmer et al., 2019; Hobart et al., 2023). These events and

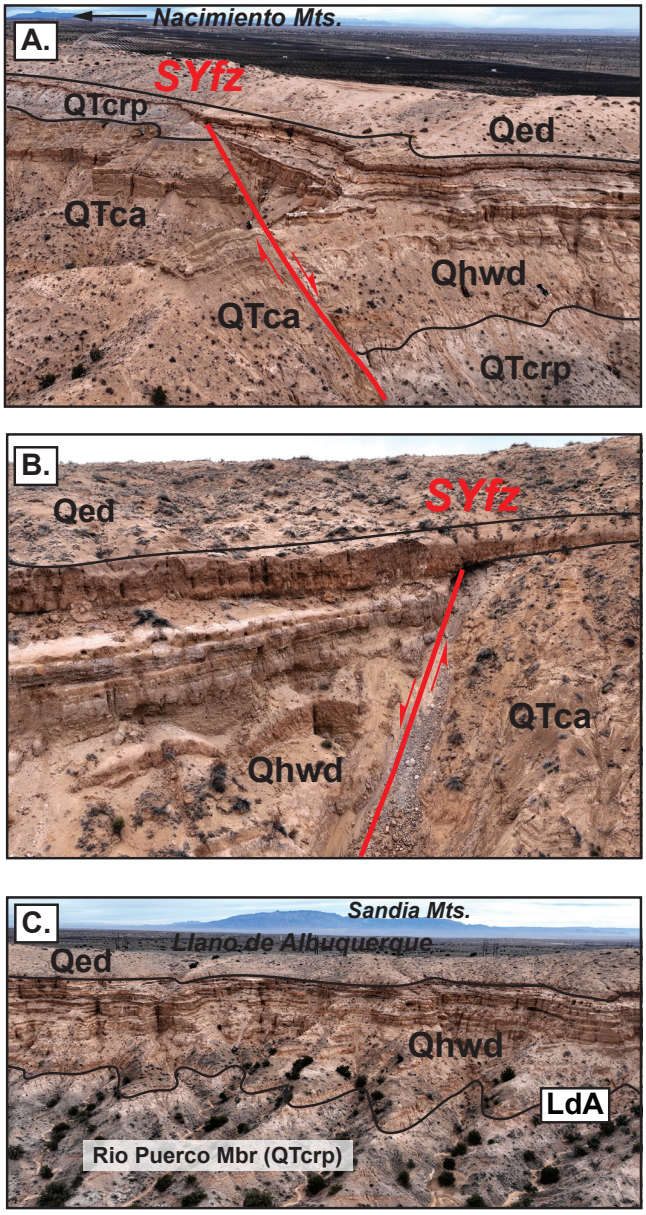


FIGURE 7. Photographs of the Calabacillas segment of the San Ysidro fault (SYfz) and hanging-wall deposits (unit Qhwd). A: View to the north of the fault juxtaposing Rio Puerco (QTcrp) and Atrisco (QTca) Members of the Ceja Formation on the left against units Qhwd and QTcrp on the right. B: View to south of the San Ysidro fault zone, showing juxtaposition of unit Qhwd on left against interbedded sandstone and mudstone of unit QTca on right. Holocene rim-capping sand dunes (Qed) bury the fault. C: View to east showing unit Qhwd overlying the white band representing the buried Llano de Albuquerque geomorphic surface (LdA) developed on the Rio Puerco Member (QTcrp).

intervening warm–cool climate transitions are expressed and superposed by paleoclimatic proxies in the southwestern United States, including dust flux, vegetation type and spatial distribution, and precipitation (as inferred from speleothem $\delta^{18}O$ data in Asmerom et al., 2010). Middle- to late-Pleistocene proxy records document local to regional climate dynamics on decadal to decamillennial timescales (Reheis et al., 2005; Asmerom et al., 2010; Fawcett et al., 2011), demonstrating that climatically influenced sediment supply and depositional trends can operate over timescales that are much shorter than long-term recurrence times estimated for faults in the Albuquerque Basin (e.g., U.S. Geological Survey, 2024). Thus, climatic variability may provide an important but indirect control on deposition in proximal hanging-wall wedges by modulating sediment supply, vegetative cover, and wind strength.

Geochronologic constraints from the underlying Ceja Formation (Connell et al., 2013) and OSL ages for upper Pleistocene deposits (Hall et al., 2008) permit comparison with paleoclimate proxy records (Fig. 9), suggesting that climatic cyclicity can strongly influence dust flux, sediment remobilization, and paleosol formation. Application of two threshold cutoffs to the $\delta^{18}O$ curve shown in Figure 9 marks the occurrence of 13 to 30 potential climatic episodes that may correspond to phases of deposition, relative geomorphic stability, and paleosol formation within this succession. Although these thresholds are arbitrary and direct paleosol-to-stage correlations have not been confirmed, the number of inferred climatic oscillations is broadly consistent with the observed stacking of multiple paleosol-bounded subunits (Fig. 9). This composite wedge architecture is therefore interpreted to reflect repeated alternations between tectonically generated accommodation and climatically forced pulses of sedimentation, reworking, and pedogenesis. We infer that these paleosols mark periods of relative stability, whereas thicker sand-dominated packages record periods of enhanced sediment flux driven by climatic variations, fault-rupture events, or both. This apparent coupling suggests that hanging-wall wedges may serve as a stratigraphic archive of the interaction among tectonic accommodation, sediment supply, and Pleistocene climate oscillations in semiarid settings. The coarse temporal resolution of these age brackets limits event-level correlations, indicating a need for higher-resolution dating of soil–stratigraphic surfaces interpreted as paleoseismic event horizons (see below).

Geochronological Refinements and Limitations

The numerous depositional events in the Calabacillas fault succession are broadly consistent with orbital-scale climate variability; however, limited internal geochronologic control precludes direct correlation of individual paleosol-bounded

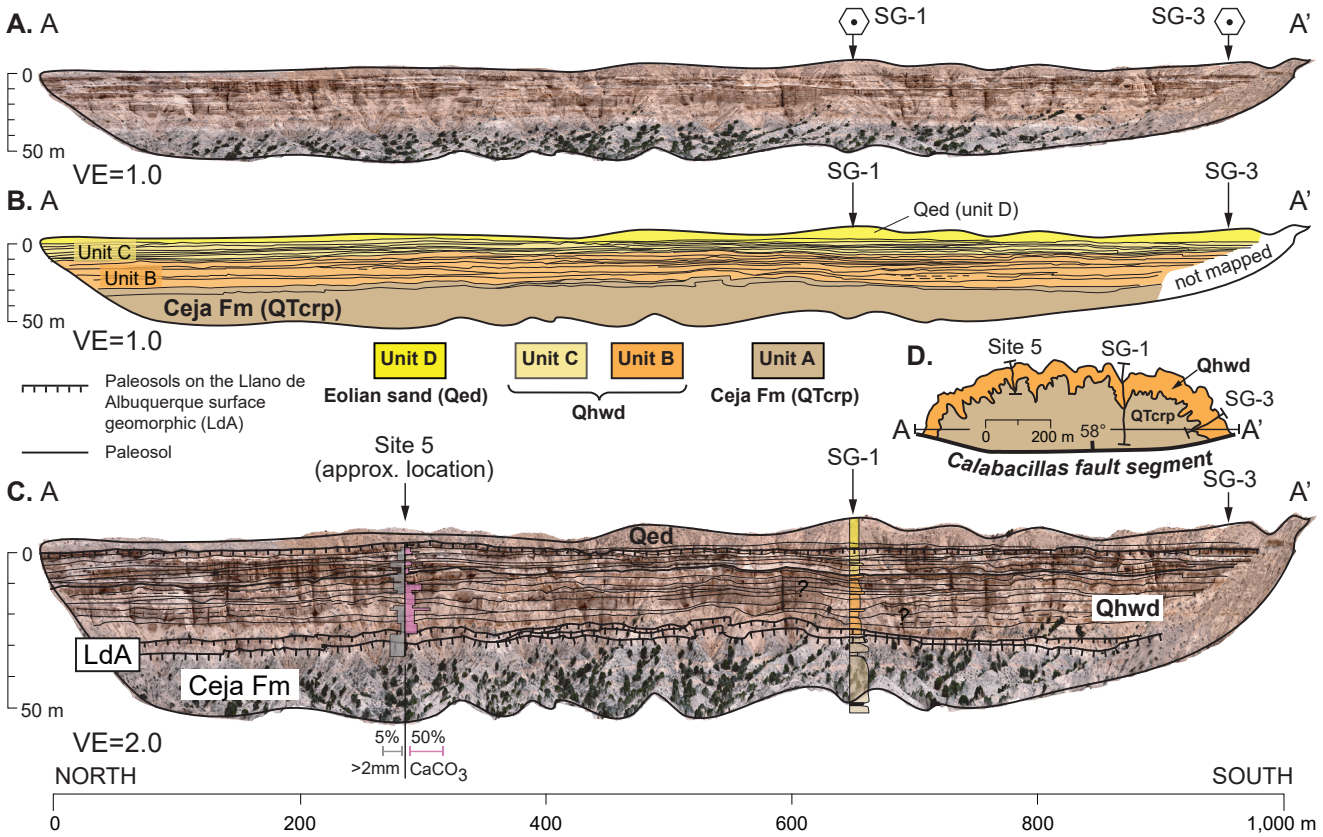


FIGURE 8. Photogrammetric model of the Calabacillas wedge (unit Qhwd). A: Uninterpreted panel from digital outcrop model (VE=1.0). B: Interpreted panel showing paleosol-bounded packages shown on stratigraphic sections SG-1 and SG-3 (VE=1.0). C: Vertically exaggerated (VE=2.0) panel highlights the lateral continuity of paleosol-bounded depositional packages, underlying paleosols correlated to the Llano de Albuquerque geomorphic surface (LdA) and overlying eolian sand (Qed). Gravel content and calcium-carbonate accumulation data from Machette et al. (1997, site 5) are projected onto the line of section. D: Simplified geologic map of amphitheater area, showing units Qhwd and QTcrp.

units to specific orbital cycles or paleoclimatic events. Refining the geochronologic control for sedimentation and paleosol development since 1.8 Ma requires an integrated, multimethod approach that can distinguish depositional ages from pedogenic overprinting. This section discusses potential dating techniques for refining the ages of fault wedges in the Albuquerque Basin.

Magnetic-polarity stratigraphy can supplement the correlation framework established by Connell et al. (2013) to confirm the 1.9–1.8 Ma Olduvai subchron elsewhere within the Ceja Formation and to identify the 0.8 Ma Brunhes–Matuyama chron boundary in overlying deposits. More detailed tephrochronology and sanidine geochronology may also provide independent age control on the SA-11 ash (see above) and fluvially reworked sanidine grains in the Ceja Formation.

Pedogenic carbonate development and soil morphology provide a useful framework for landscape-scale correlation but require calibration (e.g., Birkeland, 1999). Pedogenic carbonate accumulation rates offer additional constraints but are sensitive to climate, dust flux, and residence time, also limiting their geochronologic utility (e.g., Machette, 1985). Pedogenic carbonate can provide age constraints of soil formation. Uranium-series ($^{230}Th/^{234}U$) dating is reliable for younger systems where closed-system behavior can be reasonably assumed (e.g., Schwarcz, 1989). U-Pb methods can be used to date older (>0.5 Ma) carbonate accumulations (e.g., Aguirre Palafox et al., 2024). Both approaches may be useful for constraining the duration and timing of calcic paleosol development, but results must be interpreted in the context of open-system behavior and calcite reprecipitation.

Cosmogenic nuclide dating is another potentially useful tool for constraining depositional timing and surface exposure histories. In-situ production of cosmogenic isotopes, such as ^{10}Be and ^{26}Al in quartz, can be used to estimate burial ages of sediments and the duration of surface stability, particularly where paired-nuclide approaches allow distinction among simple exposure, inheritance, and post-depositional burial histories (e.g., Granger, 2006); however, complications related to sediment recycling, inheritance, and postdepositional mixing require careful sampling strategies and integration with independent geochronometers.

Luminescence dating also provides direct constraints on depositional timing and has been successfully used to date upper Pleistocene deposits in the region (McCalpin et al., 2011; McCalpin, 2025). Optically stimulated luminescence (OSL) dating of quartz or infrared-stimulated luminescence (IRSL) of feldspar is well suited for younger (<200 ka) eolian deposits. OSL has been successfully used on eolian deposits above the Llano de Albuquerque geomorphic surface (Hall et al., 2008). For older deposits, post-infrared IRSL (pIRIR) on feldspar grains could extend the datable range to ~500 ka, provided anomalous fading is adequately corrected (e.g., Roberts, 2008; McCalpin, 2025).

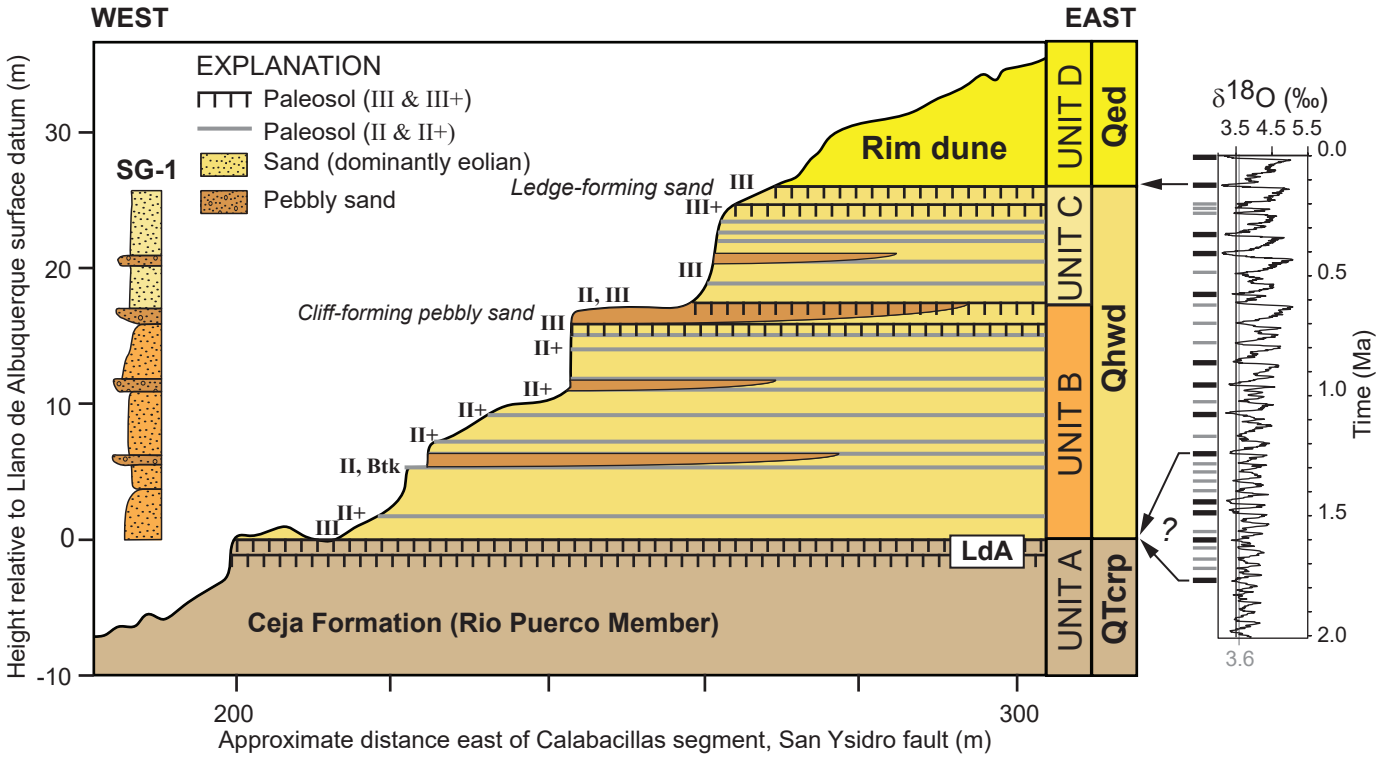


FIGURE 9. Soil–stratigraphic relationships and provisional geochronological correlations to the global paleoclimate proxy record of Lisiecki and Raymo (2015). Stratigraphic section SG-1 is projected onto a topographic profile to highlight stratigraphic interpretations of unit Qhwd. Pebbly sand lenses are shown diagrammatically. Variations in the global climate proxy record over the last two million years indicate numerous episodic shifts to drier climatic regimes that favor the development of calcic paleosols. Horizontal bars indicate the potential for climatic shifts that could promote calcic paleosol development, as inferred from cutoffs applied to the $\delta^{18}O$ curve. Thick black bars denote thresholds where the curve is less than a 3.5‰ cutoff; light-gray bars mark a slightly higher threshold of 3.6‰. Uncertainties in the maximum age of the Llano de Albuquerque geomorphic surface (LdA) are bracketed by ages discussed in Connell et al. (2013).

Paleoseismic Implications

In fault-proximal settings, climatically driven pulses of sediment interact with local tectonic accommodation generated by incremental fault displacements to produce vertically stacked, paleosol-bounded eolian packages that record alternating episodes of relatively rapid deposition and prolonged geomorphic stability and pedogenesis. Stratigraphic architecture provides a hierarchical conceptual framework for distinguishing individual depositional events within a larger composite wedge succession and cautions against interpreting each sand unit as a discrete surface-rupture event, particularly where eolian and sheetwash processes dominate sedimentation and preservation. Mapping stratigraphic relationships farther away from the fault trace can improve the distinctions between regional climatic and local tectonic signals.

As discussed above, eolian-dominated sedimentary intervals within fault-controlled sedimentary wedges may not correspond directly to discrete surface-rupturing paleoearthquake events. The presence of laterally continuous paleosols suggest regional controls on paleosol development that may be inconsistent with localized rupture-induced depositional pulses. The predominance of eolian and sheetwash deposition may obscure identification of earthquake-event horizons. Thus, these deposits likely represent compound responses to a combination of local fault-generated accommodation, climate-driven sediment supply, and relative landscape stability. Therefore, stratigraphic thickness or number of paleosol-bounded sequences may not be directly related to rupture frequency without additional independent age control to constrain individual events.

Misinterpretation of climatically controlled stratigraphic packages as paleoseismic event horizons could lead to inaccurate estimations of paleoearthquake frequency. Thus, improving the reliability of paleoseismic interpretations can benefit from more stratigraphically explicit approaches that integrate geomorphic and structural evidence for surface rupture and use independent geochronology to evaluate whether observed stratigraphic discontinuities reflect past earthquake events, climate-driven depositional pulses, or a combination of both. These observations reinforce the need to distinguish rupture-defined event horizons from climatically paced depositional pulses when interpreting the prehistoric fault record in basins with low slip rates and strong eolian overprinting.

CONCLUSIONS

Regional fault–stratigraphic relationships in the northwestern Albuquerque Basin indicate that intrabasinal normal faulting exerts a strong control on preservation and postdepositional modification of the Santa Fe Group and younger deposits. Basinward thickening of the Ceja Formation and reduced erosion of deposits above the Mio–Pliocene Rincones paleosurface reflect spatial variations in accommodation and sediment supply across the northwestern Albuquerque Basin. Footwall sections are typically thin and erosionally truncated, whereas hanging-wall successions preserve thicker and more complete stratigraphic records due to enhanced preservation.

Continued intrabasinal faulting following the cessation of regional Santa Fe Group basin filling is recorded by fault-controlled hanging-wall wedges above the Llano de Albuquerque geomorphic surface. This transition marks a shift from widespread fluvial deposition to more localized eolian, sheetwash, and colluvial deposition, reflecting increased structural partitioning of sediment accumulation.

Fault-controlled hanging-wall wedge deposits along the Calabacillas segment of the San Ysidro fault zone record a composite stratigraphic succession produced by the interaction of incremental fault displacement, climatically modulated sedimentation, and pedogenesis. A 26-m (85-ft)-thick succession containing more than 18 paleosol-bounded subunits reflects repeated alternations between relatively short-lived depositional pulses and prolonged intervals of landscape stability for over one million years. The predominance of eolian and sheetwash sedimentation, together with the development of laterally continuous, cumulic paleosols, indicates strong climatic controls on sediment supply, accumulation, and preservation.

These findings have important implications for paleoseismic analysis in semiarid basins with low rates of vertical fault slip. Misinterpretation of climatically controlled stratigraphic packages as paleoseismic event horizons may lead to inaccurate estimates of paleoearthquake frequencies. More robust paleoseismic reconstructions can benefit from an integrated analysis of sedimentology, soil–stratigraphic architecture, sediment provenance, and high-resolution geochronology to distinguish tectonically generated deposition from climatically modulated sediment pulses. Recognition of the combined influence of tectonic and climatic processes is essential for accurately identifying individual ground-rupture events and reconstructing Pleistocene earthquake histories in semiarid, eolian-influenced basins with low rates of tectonic deformation.

ACKNOWLEDGMENTS

This contribution was based on geologic mapping of the Albuquerque–Rio Rancho metropolitan area for the New Mexico STATEMAP Program. We thank the New Mexico State Land Office for access to the Calabacillas fault site. Steve Rogers assisted with descriptions of RH-1 and SG-1 stratigraphic sections. The authors benefited from discussions with Bruce Harrison, John Hawley, Dave Love, Jim McCalpin, and Susan Olig. We thank Grant Meyer, Les McFadden, and Zachary Lifton for their thoughtful comments and constructive suggestions.

REFERENCES

Aguirre Palafox, L.E., Möller, A., McLean, N.M., Ludvigson, G.A., Colombi, C.E., and Montañez, I.P., 2024, U-Pb geochronology of paleosol carbonate cements by LA-ICP-MS: A proof of concept and strategy for dating the terrestrial record: Geochemistry, Geophysics, Geosystems, v. 25, no. 6, e2024GC011488. https://doi.org/10.1029/2024GC011488

Asmerom, Y., Polyak, V.J., and Burns, S.J., 2010, Variable winter moisture in the southwestern United States linked to rapid glacial climate shifts: Nature Geoscience, v. 3, p. 114–117. https://doi:10.1038/ngeo754

Birkeland, P.W., 1999, Soils and geomorphology (third edition): New York, Oxford University Press, 430 p.

Connell, S.D., 2004, Geology of the Albuquerque basin and tectonic development of the Rio Grande rift in north-central New Mexico, *in* Mack, G.H., and Giles, K.A., eds., The Geology of New Mexico: A Geologic History: New Mexico Geological Society, Special Publication 11, p. 359–388. https://doi.org/10.56577/SP-11

Connell, S.D., 2006, Preliminary geologic map of the Albuquerque-Rio Rancho metropolitan area and vicinity, Bernalillo and Sandoval Counties, New Mexico: New Mexico Bureau of Geology and Mineral Resources, Open-file report 496, scale 1:50,000. https://doi.org/10.58799/OFR-496

Connell, S.D., 2008a, Geologic map of the Albuquerque-Rio Rancho metropolitan area, Bernalillo and Sandoval County, New Mexico: New Mexico Bureau of Geology and Mineral Resources, Geologic Map GM-78, scale 1:50,000, 2 pls. https://doi.org/10.58799/GM-78

Connell, S.D., 2008b, Refinements to the stratigraphic nomenclature of the Santa Fe Group, northwestern Albuquerque basin, New Mexico: New Mexico Geology, v. 30, no. 1, p. 14–35. https://doi.org/10.58799/NMG-v30n1.14

Connell, S.D., Koning, D.J., and Cather, S.M., 1999, Revisions to the stratigraphic nomenclature of the Santa Fe Group, northwestern Albuquerque basin, New Mexico: New Mexico Geological Society, Guidebook 50, p. 337–353. https://doi.org/10.56577/FFC-50.337

Connell, S.D., Smith, G.A., Geissman, J.W., and McIntosh, W.C., 2013, Climatic controls on nonmarine depositional sequences in the Albuquerque Basin, Rio Grande rift, north-central New Mexico, *in* Hudson, M.R., and Grauch, V.J.S., eds., New Perspectives on Rio Grande Rift Basins: From Tectonics to Groundwater: Geological Society of America Special Paper 494, p. 383–425. https://doi:10.1130/2013.2494(15)

Ellwein, A.L., Mahan, S.A., and McFadden, L.D., 2015, Impacts of climate change on the formation and stability of late Quaternary sand sheets and falling dunes, Black Mesa region, southern Colorado Plateau, USA: Quaternary International, v. 362, p. 87–107. https://doi.org/10.1016/j.quaint.2014.10.015

Ellwein, A.L., McFadden, L.D., McAuliffe, J.A., and Mahan, S.A., 2018, Late Quaternary soil development enhances aeolian landform stability, Moenkopi Plateau, southern Colorado Plateau, USA: Geosciences, v. 8, no. 5, 146, 29 p. https://doi.org/10.3390/geosciences8050146

Farmer, J.R., Hönisch, B., Haynes, L.L., Jung, S., Ford, H.L., Raymo, M.E., Jaume-Seguí, M., Bell, D.B., Goldstein, S.L., Pena, L.D., Yehudai, M., and Kim, J., 2019, Deep Atlantic Ocean carbon storage and the rise of 100,000-year glacial cycles: Nature Geoscience, v. 12, p. 355–360. https://doi:10.1038/s41561-019-0334-6

Fawcett, P.J., et al., 2011, Extended megadroughts in the southwestern United States during Pleistocene interglacials: Nature, v. 470, p. 518–521. https://doi:10.1038/nature09839

Gibbard, P.L., and Head, M.J., 2020, The Quaternary Period, *in* Gradstein, F.M., Ogg, J.G., Schmitz, M.D., and Ogg, G.M., eds., Geologic Time Scale 2020, v. 2, p. 1217–1255. https://doi.org/10.1016/B978-0-12-824360-2.00030-9

Granger, D.E., 2006, A review of burial dating methods using ^{26}Al and ^{10}Be, *in* Alonso-Zara, A.M., and Tanner, L.H., eds., In Situ-Produced Cosmogenic Nuclides and Quantification of Geological Processes: Geological Society of America Special Paper 415, p. 1–16. https://doi.org/10.1130/2006.2415(01)

Gray, H., DuRoss, C., Nicovich, S., and Gold, R., 2022, Luminescence sediment tracing reveals the complex dynamics of colluvial wedge formation: Science Advances, v. 8, no. 22, eabo0747. https://doi:10.1126/sciadv.abo0747

Hall, S.A., Goble, R.G., and Raymon, G.R., 2008, OSL ages of upper Quaternary eolian sand and paleosols, northwest Albuquerque Basin, New Mexico: New Mexico Geology, v. 30, no. 2, p. 39–49. https://doi.org/10.58799/NMG-v30n2.39

Hobart, B., Lisiecki, L.E., Rand, D., Taehee, L., and Lawrence, C.E., 2023, Late Pleistocene, 100-kyr glacial cycles paced by precession forcing of summer insolation: Nature Geoscience, v. 16, p. 717–722. https://doi:10.1038/s41561-023-01235-x

Holliday, V.T., Huckell, B.B., Mayer, J.H., Forman, S.L., and McFadden, L.D., 2006, Geoarchaeology of the Boca Negra Wash Area, Albuquerque Basin, New Mexico, USA: Geoarchaeology, v. 21, no. 8, p. 756–802. https://doi.org/10.1002/gea.20139

Kelley, V.C., 1977, Geology of the Albuquerque basin, New Mexico: New Mexico Bureau of Mines and Mineral Resources, Memoir 33, 60 p. https://doi.org/10.58799/M-33

Koning, D.J., Martin, L., Zimmerer, M., Mamer, E., Doherty, A., and Sturgis, L., 2026, Investigation of Hydrostratigraphic Units of the Santa Fe Group Aquifer in the Northwestern Albuquerque Basin, New Mexico: New Mexico Bureau of Geology and Mineral Resources, Open-file Report 635, 76 p. https://doi.org/10.58799/OFR-635

Lisiecki, L.E., and Raymo, M.E., 2015, A Pliocene–Pleistocene stack of 578 globally distributed benthic δ^{18}O records: Paleoceanography, v. 20, PA1003, 17 p. https://doi:10.1029/2004PA001071

Machette, M.N, 1978, Dating Quaternary faults in the southwestern United States by using buried calcareous paleosols: U.S. Geological Survey Journal of Research, v. 6, p. 369–381.

Machette, M.N., 1985, Calcic soils of the southwestern United States, *in* Weide, D. L., ed., Soils and Quaternary Geology of the Southwestern United States: Geological Society of America Special Paper 203, p. 1–21. https://doi.org/10.1130/SPE203-p1

Machette, M.N., Long, T., Bachman, G.O., and Timbel, N.R., 1997, Laboratory data for calcic soils in central New Mexico: Background information for mapping Quaternary deposits in the Albuquerque Basin: New Mexico Bureau of Mines and Mineral Resources, Circular 205, 63 p. https://doi.org/10.58799/C-205

McCalpin, J.P., 1996, Chapter 2, Field techniques in paleoseismology, *in* McCalpin, J.P., ed., Paleoseismology: International Geophysics, v. 62, p. 33–83. https://doi.org/10.1016/S0074-6142(96)80069-6

McCalpin, J.P., 2025, Paleoseismology of the Zia fault and its impact on seismic hazard for Albuquerque, New Mexico, USA: Engineering and Environmental Geosciences, v. 31, no. 1, p. 37–50. https://doi.org/10.21663/EEG-D-24-00037

McCalpin, J.P., Olig, S.S., Harrison, J.B.J., and Berger, G.W., 2006, Quaternary faulting and soil formation on the County Dump fault, Albuquerque, New Mexico: New Mexico Bureau of Geology and Mineral Resources, Circular 212, 36 p. https://doi.org/10.58799/C-212

McCalpin, J.P., Harrison, J.B.J., Berger, G.W., and Tobin, H.C., 2011, Paleoseismicity of a low-slip-rate normal fault in the Rio Grande rift, USA: The Calabacillas fault, Albuquerque, New Mexico, *in* Audemard, F.A., Michetti, A.M., and McCalpin, J.P., eds., Geological Criteria for Evaluating Seismicity Revisited: Forty Years of Paleoseismic Investigations and the Natural Record of Past Earthquakes: Geological Society America Special Paper 479, p. 23–46. https://doi.org/10.1130/2011.2479(01)

Nelson, A.R., 1992, Lithofacies analysis of colluvial sediments—An aid in interpreting the recent history of Quaternary normal faults in the Basin and Range province, Western United States: Journal of Sedimentary Research, v. 62, no. 4, p. 607–621. https:// doi: 10.1306/D426796F-2B26-11D7-8648000102C1865D

Pederson, J., Pazzaglia, F., and Smith, G., 2000, Ancient hillslope deposits: Missing links in the study of climate controls on sedimentation: Geology, v. 28, no. 1, p. 27–30. https://doi.org/10.1130/0091-7613(2000)028<0027:AHDMLI>2.3.CO;2

Pederson, J., Smith, G., and Pazzaglia, F., 2001, Comparing the modern, Quaternary, and Neogene records of climate-controlled hillslope sedimentation in southeast Nevada: Geological Society of America Bulletin, v. 113, no. 3, p. 305–319. https://doi.org/10.1130/0016-7606(2001)113<0305:CTMQAN>2.0.CO;2

Personius, S.F., and Mahan, S.A., 2003, Paleoearthquakes and eolian-dominated fault sedimentation along the Hubbell Spring fault zone near Albuquerque, New Mexico: Bulletin of the Seismological Society of America, v. 93, no. 3, p. 1355–1369. https://doi.org/10.1785/0120020031

Pye, K., and Tsoar, H., 2009, Aeolian Sand and Sand Dunes: Berlin, Springer-Verlag, 458 p. https://doi.org/10.1007/978-3-540-85910-9

Reheis, M.C., Reynolds, R.L., Goldstein, H., Roberts, H.M., Yount, J.C., Axford, Y., Cummings, L.S., and Shearin, N., 2005, Late Quaternary eolian and alluvial response to paleoclimate, Canyonlands, southeastern Utah: Geological Society of America Bulletin, v. 117, no. 7–8, p. 1051–1069. https://doi:10.1130/B25631.1

Roberts, H.M., 2008, The development and application of luminescence dating to loess deposits: A perspective on the past, present and future: Boreas, v. 37, p. 483–507. https://doi.org/10.1111/j.1502-3885.2008.00057.x

Schwarcz, H.P., 1989, Uranium series dating of Quaternary deposits: Quaternary International, v. 1, p. 7–17. https://doi.org/10.1016/1040-6182(89)90005-0

Tedford, R.H., and Barghoorn, S.F., 1999, Santa Fe Group (Neogene), Ceja del Rio Puerco, northwestern Albuquerque Basin, Sandoval County, New Mexico: New Mexico Geological Society, Guidebook 50, p. 327–335. https://doi.org/10.56577/ffc-50.327

Thompson, R.A., Shroba, R.R., Menges, C., Schmidt, W.L., Personius, S.F., and Brandt, T.R., 2009, Geologic map of The Volcanoes quadrangle, Bernalillo and Sandoval Counties, New Mexico: U.S. Geological Survey, Scientific Investigations Report 3083, 1 sheet, scale 1:24,000. https://doi.org/10.3133/sim3083

U.S. Geological Survey, 2024, Quaternary fault and fold database for the United States: U.S. Geological Survey and New Mexico Bureau of Mines and Mineral Resources. https://www.usgs.gov/natural-hazards/earthquake-hazards/faults (accessed December 2025).

Westoby, M.J., Brasington, J., Glasser, N.F., Hambrey, M.J., and Reynolds, J.M., 2012, Structure-from-motion photogrammetry: A low-cost, effective tool for geoscience applications: Geomorphology, v. 179, p. 300–314. https://doi.org/10.1016/j.geomorph.2012.08.021

Wright, H.E., Jr., 1946, Tertiary and Quaternary geology of the Lower Rio Puerco area, New Mexico: Geological Society of America Bulletin, v. 57, no. 5, p. 383–456. https://doi.org/10.1130/0016-7606(1946)57[383:TAQGOT]2.0.CO;2



Aerial view from the Ceja del Rio Puerco, looking east across the Llano de Albuquerque toward the Sandia Mountains. Photograph courtesy of Sean Connell.